Raindrop shape determined by computing steady axisymmetric solutions for Navier-Stokes equations

James Q. Feng * and Kenneth V. Beard**

*Boston Scientific Corporation, 3 Scimed Place, Maple Grove, Minnesota

E-mail:james.feng@bsci.com

**Atmospheric Physics Associates, Savoy, Illinois

1. Introduction

The shape of raindrops is of fundamental interest to atmospheric scientists, playing an essential role in the remote measurement of rainfall rate and nowcasting of precipitation. Not surprisingly, numerous publications in the literature have been devoted to determining the raindrop shape by both experimental and theoretical approaches. The study of the shape of water drops falling in air apparently began with the experiments of Lenard (1904), who speculated that a balance between the centrifugal pressure due to internal circulation and surface tension at the drop surface played the key role in drop deformation. Early efforts with high-speed photography (cf. Flower 1928; Edgerton and Killian 1939; Blanchard 1948, 1950; Magono 1954) showed that a large water drop (of diameter > 2 mm) falling at terminal velocity tends to take a shape of a hamburger bun with a flattened bottom and a curved dome top[1]. But the reported drop shapes by different authors for a given drop size would differ considerably due to various experimental difficulties until Pruppacher and Beard (1970); Pruppacher and Pitter (1971) developed a refined vertical wind tunnel to freely suspend water drops in the upward air stream and to obtain detailed information on axis ratio with high-quality photographs as a function of raindrop size.

It has generally been recognized that a water drop of diameter $d < 1$ mm has nearly spherical shape due to the strong surface tension effect at the water-air interface, with the relative air flow outside and liquid circulation inside of the drop being basically laminar, steady, and axisymmetric. The drops with noticeable deformations from the spherical shape are those having diameters $d > 1$ mm, which typically oscillate when falling in air while the shedding of vortices occurs in the unstable wake (Pruppacher and Klett 1978; Beard, Ochs, and Kubesh 1989; Szakáll et al. 2009). Thus, the raindrop deformations of any practical significance are essentially transient in nature, oscillating around an 'equilibrium' shape. The raindrop shape, as usually being referred to, is actually this steady axisymmetric equilibrium shape, unless the attention is particularly focused on the dynamics of drop oscillations (e.g., Beard, Ochs, and Kubesh 1989; Feng and Beard 1991; Szakáll et al. 2009).

In principle, the steady axisymmetric equilibrium shape of a drop falling in air can be theoretically determined by evaluating the traction boundary condition that includes interfacial stresses from (steady axisymmetric) fluid flows both external and internal to the drop as well as the hydrostatic pressure due to gravity (e.g., Feng 2010). However, rigorous as it may seem, this effort requires detailed knowledge about the flow fields in both the air phase outside and water phase inside of the drop, which is not easily accessible without performing sophisticated numerical computations to solve the nonlinear Navier-Stokes equations especially at Reynolds number > 300 for noticeable drop deformations. But the steady axisymmetric flow field at Reynolds number > 300 is known to be unstable; the observations typically show transient vortex shedding in the wake (Pruppacher and Klett 1978; Clift, Grace, and Weber 1978). Therefore, a truly rigorous theoretical approach to the raindrop shape problem is expected to involve numerical computations of transient fully three-dimensional solutions to the nonlinear Navier-Stokes equations, and then to extract the steady axisymmetric equilibrium shape through time-smoothing over a large number of solutions at different time steps (similar to the experimental approach of Szakáll et al. (2009) through a histogram analysis.)

Interestingly though, several previous theoretical attempts with incomplete account for the stress distribution at the drop surface yielded amazingly accurate results for the axis ratio as well as detailed drop shape for various drop sizes when compared with the experimental results (e.g., Pruppacher and Pitter

[1] actually quite different from those 'raindrops' of teardrop shapes often illustrated in popular culture and even on the TV news channels for a coming storm

1971; Green 1975; Beard and Chuang 1987; Beard, Feng, and Chuang 1989). Among others, the most intriguing method might be that of Green (1975) who determined axis ratios by balancing the hydrostatic pressure and surface tension with local curvatures at the equator of an oblate spheroid, with the flow effect completely ignored. Restricted by the assumption of drops with an oblate spheroidal shape, however, Green (1975) could not provide detailed description of the drop shape with flattened bottom and rounded top–asymmetric to the equatorial plane, though his axis ratio agrees surprisingly well with the experiments and more sophisticated models (cf. Beard, Feng, and Chuang 1989). Apparently, the mathematical formulation of this spheroid model is not limited to small drop deformation. But its assumption of a constant excess pressure inside the drop independent of drop deformation is not consistent with the reality.

A mathematically more reasonable model for the raindrop shape seems to be that originated from Savic (1953), later improved by Pruppacher and Pitter (1971) and then formalized in terms of first-order domain perturbation theory by Beard, Feng, and Chuang (1989). This was a model established upon the linearized Young-Laplace equation describing the local balance between surface curvatures with surface tension and pressure difference distribution across the interface, but the viscous normal stresses arising from fluid flow were not considered. As consistent with the regular perturbation procedure, the first-order drop surface deformation was determined by the difference between the aerodynamic pressure (e.g., that measured by Fage 1937, at the surface of a rigid sphere for large Reynolds number flow) outside the drop surface and the hydrostatic pressure inside a spherical drop. The results of this perturbation model turned out to be quite accurate especially for smaller drops (e.g., those with $d < 4$ mm) with deformations not too far from the spherical base shape, just as one would mathematically expect from the perturbation theory.

To remove the restriction for small drop deformation, Beard and Chuang (1987) iteratively solved the full nonlinear Young-Laplace equation by numerical means, using an internal hydrostatic pressure with an external aerodynamic pressure based on measurements for a sphere but adjusted for the effect of free surface distortion and drag force magnitude. Physically, the numerical model of Beard and Chuang (1987) contained basically the same ingredients as that in the perturbation models of Pruppacher and Pitter (1971), Beard, Feng, and Chuang (1989), etc. But mathematically it became applicable to very large raindrops with substantial deformations. To date, all the experimentally measured equilibrium drop shapes have shown to agree very well with those predicted by Beard and Chuang (1987) (cf., Szakáll et al. 2009; Beard, Bringi, and Thurai 2010). Noteworthy here is that in the model of Beard and Chuang (1987) the external pressure distribution was not determined self-consistently from the first principles; rather it relied on an assumption that the fractional deviation of the adjusted pressure distribution from that of Fage (1937) would be the same as the fractional deviation in potential flow around an oblate spheroid from a sphere and with an amplitude factor for adjusting the drag force to balance the drop weight, the validity of which is still open for verification.

Nevertheless, the impressive success of those approximate, seemingly incomplete models (by considering only the external aerodynamic pressure and internal hydrostatic pressure) in describing the raindrop shape suggests that

- The viscous stresses could be relatively unimportant compared with the dynamic pressure;
- The dynamic normal stress due to internal circulation might be negligible;
- Models much simpler than that involving the transient fully three-dimensional solutions to the Navier-Stokes equations might be adequate enough.

The purpose of the present work is to examine the possibility of using the computed steady axisymmetric solutions of the Navier-Stokes equations (as in Feng 2010) to determine the (equilibrium) raindrop shape. If successful, this approach allows inclusion of almost all the basic physical ingredients with the flow field and free surface shape being determined simultaneously, and thereby many *ad hoc* assumptions employed in the previous approximate raindrop shape models can be eliminated.

2. Governing equations

As described in Feng (2010), here we consider a liquid (water) drop of volume $\frac{4}{3}\pi R^3$, constant density ρ_l, viscosity μ_l, and surface tension γ, falling through a gas (air) of constant density ρ_g and viscosity μ_g, in a gravitational field with a constant acceleration of gravity g. For convenience of analysis, all the variables and parameters are made dimensionless by measuring length in units of the volume-equivalent drop radius R, fluid flow velocity $\boldsymbol{v}$ in units of drop's terminal velocity U, and pressure p in units of $\mu_g U/R$. By measuring fluid density in units of ρ_g and viscosity in units of μ_g, the dimensionless liquid density and viscosity are respectively denoted by ρ ($\equiv \rho_l/\rho_g$) and μ ($\equiv \mu_l/\mu_g$), while those for the surrounding gas becoming unity. A

reference frame moving with the liquid drop is adopted here with the coordinate origin fixed at the centre of mass of the drop. Then, the axisymmetric, laminar flow inside and outside of the drop is governed by the steady incompressible Navier-Stokes equations

$$\frac{\rho}{2} Re\, \boldsymbol{v}\cdot\boldsymbol{\nabla}\boldsymbol{v} = \boldsymbol{\nabla}\cdot\boldsymbol{T}_l \ \text{ with } \ \boldsymbol{T}_l \equiv -p\boldsymbol{I}+\mu[\boldsymbol{\nabla}\boldsymbol{v}+(\boldsymbol{\nabla}\boldsymbol{v})^T]\,, \tag{1}$$

and

$$\frac{1}{2} Re\, \boldsymbol{v}\cdot\boldsymbol{\nabla}\boldsymbol{v} = \boldsymbol{\nabla}\cdot\boldsymbol{T}_g \ \text{ with } \ \boldsymbol{T}_g \equiv -p\boldsymbol{I}+\boldsymbol{\nabla}\boldsymbol{v}+(\boldsymbol{\nabla}\boldsymbol{v})^T\,, \tag{2}$$

where Re denotes the Reynolds number defined as $2\rho_g U R/\mu_g$, $\boldsymbol{I}$ the identity tensor, superscript 'T' stands for the transpose, and the incompressible flow velocity $\boldsymbol{v}$ satisfies the continuity equation $\boldsymbol{\nabla}\cdot\boldsymbol{v}=0$.

A cylindrical (z,r)-coordinate system is used here with the z-axis coinciding with the axis of symmetry and pointing in the opposite direction as that of the gravitational field. Thus, at the drop's free surface S_f conservation of momentum is satisfied by imposing the traction boundary condition

$$\boldsymbol{n}\cdot(\boldsymbol{T}_g-\boldsymbol{T}_l) = \frac{1}{Ca}\left(\frac{d\boldsymbol{t}}{ds}+\frac{\boldsymbol{n}}{r}\frac{dz}{ds}\right)-p_a\boldsymbol{n}+St\,z\,\boldsymbol{n} \ \text{ on } S_f\,, \tag{3}$$

where $Ca \equiv \mu_g U/\gamma$ is the capillary number. The local unit normal vector $\boldsymbol{n}$ at the free surface points from the gas into liquid, and the local unit tangent vector $\boldsymbol{t}$ points in the direction of increasing s (from the front stagnation point) along the free surface and relates to $\boldsymbol{n}$ in such a way that $\boldsymbol{n}\times\boldsymbol{t}=\boldsymbol{e}_\theta$ (with the right-handed cylindrical coordinate system (z,r,θ) being used in the present work).

The constant excess pressure inside the drop p_a is solved as an unknown to satisfy an overall constraint that the volume enclosed by the free surface S_f remains constant

$$\int_{S_f} r^2\,\frac{dz}{ds}\,ds = \frac{4}{3}\,, \tag{4}$$

where the Stokes number $St \equiv (\rho-1)\rho_g\, g\, R^2/(\mu_g U)$, representing the ratio of buoyancy force and viscous force, is also solved as an unknown to satisfy another overall constraint that the drop's centre of mass remains at the coordinate origin

$$\int_{S_f} z\, r^2\,\frac{dz}{ds}\,ds = 0\,. \tag{5}$$

As might be noted, the gravitational (body) force term does not explicitly appear in (1) and (2) because the hydrostatic pressure in the bulk liquid has been lumped in the generalized pressure p. Hence, the hydrostatic pressure effect due to buoyancy force only appears in the boundary condition (3) through St.

Moreover, the flow velocity field must satisfy

$$\boldsymbol{n}\cdot\boldsymbol{v} = 0 \quad \text{on } S_f \text{ and } r=0\,, \tag{6}$$

at the free surface S_f, due to the kinematic condition, and at the axis of symmetry ($r=0$), as required by the symmetry condition. In addition, the stress-free symmetric condition at the axis of symmetry ($r=0$) can be expressed as

$$\boldsymbol{e_z e_r} : \boldsymbol{T} = 0 \quad \text{at} \quad r=0\,, \tag{7}$$

where $\boldsymbol{e_z}$ and $\boldsymbol{e_r}$ denote the unit vectors in the $z-$ and $r-$directions, respectively. (Here $\boldsymbol{T}$ without the subscript 'l' or 'g' stands for the hydrodynamic stress tensor in both phases.)

Among several treatments of the far-field boundaries, the simplest way for the present problem is to consider a cylindrical container wall with large enough radius (e.g., $10\times R$) with its centerline coinciding with the axis of symmetry of the falling liquid drop. Thus, at the cylindrical container wall ($r=10$) and the upstream (or 'inlet') boundary (e.g., located at $z=-10$ in Figure 1), the Dirichlet type of condition for uniform flow velocity is specified as

$$\boldsymbol{v} = \boldsymbol{e_z} \quad \text{on } \ r=10 \text{ and } \ S_{inlet}\,. \tag{8}$$

At the downstream (or 'outflow') boundary (e.g., located at $z=15$ in Figure 1), fully-developed flow condition for hydrodynamic stresses is used, i.e.,

$$\boldsymbol{e_z e_r} : \boldsymbol{T}_g = \frac{\partial v_z}{\partial r} \ \text{ and } \ \boldsymbol{e_z e_z} : \boldsymbol{T}_g = 0 \quad \text{on } \ S_{outlet}\,. \tag{9}$$

As in Feng (2010), the mathematical system (1)-(9) contains a complete set of equations and boundary conditions for accurately determining the steady fluid mechanics behavior of a liquid drop falling through a quiescient gas. By simply including an additional term associated with $\partial\boldsymbol{v}/\partial t$ on the left side of (1) and (2) and adding a time-derivative term in the kinematic condition (6), the system can describe the transient fluid flow problems, too. The Reynolds number Re, capillary number Ca, (dimensionless) liquid density ρ, and (dimensionless) liquid viscosity μ are the four independent parameters that can be conveniently specified[2], with St determined as part of the solution. Once Re, Ca, ρ, μ, and St are given, other relevant dimensionless parameters associated with a solution can all be calculated in terms of them. For example, the drag

[2] According to the findings of Feng (2010), however, it seems the combined parameter ρ/μ^2 controls the basical behavior of a liquid drop falling in gas; therefore, ρ and μ may not be considered as completely independent

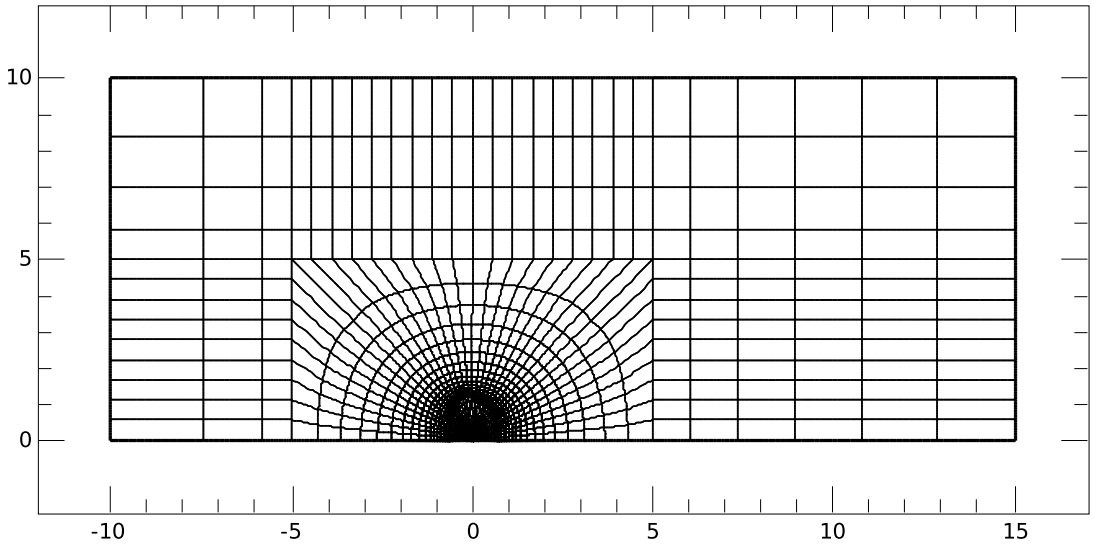

FIG. 1. Finite-element mesh of the problem domain (as exemplified by the case of $\rho = 1000$, $\mu = 100$, $Re = 500$, and $We = 15$).

coefficient C_D, Weber number We, Ohnesorge number Oh, Morton number Mo, and Eötvös number Eo (which is also called Bond number Bo) can be evaluated according to

$$\begin{aligned} C_D &\equiv 8R\,g\,(\rho-1)/(3\,U^2) = 16St/(3Re)\,, \\ We &\equiv 2\rho_g\,U^2\,R/\gamma = Re\,Ca\,, \\ Oh &\equiv \mu_l/\sqrt{2\rho_l\,\gamma\,R} = \mu\sqrt{We/\rho}\,/Re\,, \\ Mo &\equiv g\,\mu_g^4(\rho-1)/(\rho_g\,\gamma^3) = 3\,C_D\,We^3/(4Re^4)\,, \\ Eo &\equiv 4\,(\rho-1)\rho_g\,g\,R^2/\gamma = 3\,C_D\,We/4 = Mo\,Re^4/We^2. \end{aligned} \tag{10}$$

By virtue of dynamical similarity (as discussed by Batchelor (1967)), each solution to the nondimensional governing equations for a set of specified Re, Ca, ρ, and μ can represent numerous seemingly different fluid systems and drop sizes.

It should be noted that the traction boundary condition (3) is in a vector form. If a dot (or scalar) product with the unit normal vector $\boldsymbol{n}$ is performed on both sides (cf., Aris 1962), (3) would be turned into a scalar equation of the form very similar to that of the Young-Laplace equation (as used by many previous authors for various raindrop shape models), except standing on left side is $\boldsymbol{nn}\!:\!(\boldsymbol{T}_g - \boldsymbol{T}_l)$ instead of just the pressure difference across the free interface. Actually, the term $\boldsymbol{nn}\!:\!(\boldsymbol{T}_g - \boldsymbol{T}_l)$ is the complete dynamic *normal stress* difference across the free interface, containing both the pressure and viscous normal stress associated with fluid flow. Thus, all previous raindrop shape models (e.g., Savic 1953; Pruppacher and Pitter 1971; Beard and Chuang 1987; Beard, Feng, and Chuang 1989) only partially accounted for the fluid flow effects, taking the aerodynamic pressure (based on that measured for spheres–the best available data) to approximate the term $-\boldsymbol{nn}\!:\!\boldsymbol{T}_g$ and completely ignoring the term $\boldsymbol{nn}\!:\!\boldsymbol{T}_l$ as a consequence of the internal circulation (apparently for lack of knowledge). These *ad hoc* approximations for the normal stresses in previous raindrop shape models are eliminated naturally in the present mathematical framework. All the dynamic stress terms and the shape of deformable drop surface can now be determined simultaneously in a self-consistent fashion.

3. Computational technique

As demonstrated by (Feng 2010, as well as several citations therein), solutions to this type of free-boundary problem can be computed by discretizing the partial differential equation system (1)-(9) with the Galerkin's method of weighted residuals using finite-element basis functions (cf., Strang and Fix 1973; Kistler

and Scriven 1983)[3]. In doing so, the problem domain is divided into a set of quadrilateral elements (cf. figure 1), with biquadratic basis functions being used for expanding the velocity field and linear discontinuous basis functions for pressure. The distribution of finite-element mesh points around the deformable free surface is determined by a pair of elliptic partial differential equations that are also be descretized by the Galerkin finite-element method (cf., Christodoulou and Scriven 1992; de Santos 1991). Then, the set of nonlinear algebraic equations of Galerkin's weighted residuals is simultaneously solved by Newton's method of iterations (Ortega and Rheinoldt 1970). At each Newton iteration, the Jacobian matrix of sensitivities of residuals to unknowns is evaluated with the values of unknowns determined in the previous iteration. The resulting linear algebra system is then solved by direct factorization of the Jacobian matrix with a modified version of Hood's frontal solver (Hood 1976). The iteration is continued until the L_2 norm of residual vector becomes less than 10^{-8}. It usually takes no more than five or six iterations to obtain a converged solution, by virtue of the quadratic convergence rate of the Newton iteration scheme.

Because successful solution of nonlinear equations by Newton iterations relies on sufficiently accurate initial estimates of the solution, it is often convenient to start the solution procedure by computing cases with diminshingly weak nonlinearities at small Ca (or We) and Re for nearly spherical drops. Once a solution for a given set of parameters is obtained, it can be used as an effective initial estimate for another nearby solution corresponding to one or more parameters being varied slightly in the parameter space. Thus, solutions for almost any set of parameters, if exist, can be computed by varying the parameters in small steps from a 'first' solution through numerical continuation.

4. Results

Before performing any computation, we need to specify the values of ρ and μ, among others. It is known that ρ_g for air is a function of the air pressure and temperature. If we consider the air pressure to be fixed at 1.013×10^5 Pa (i.e., 1 atm–a standard condition at the surface of earth), the dry air density can be 1.292 kg/m^3 at 0^oC, or 1.247 kg/m^3 at 10^oC or 1.204 kg/m^3 at 20^oC, and so on. But for water, its density merely varies from 1000 kg/m^3 at 0^oC to 998 kg/m^3 at 20^oC. Hence without loss of generality, assuming $\rho = 800$ (i.e., $\rho_g = 1.25$ kg/m^3 taken at 10^oC) for water drop in air can be quite reasonable. The fluid viscosity depends on temperature, too. For example, the viscosity of water is 1.79×10^{-3} N s/m^2 at 0^oC, 1.30×10^{-3} N s/m^2 at 10^oC, 1.00×10^{-3} N s/m^2 at 20^oC, 7.98×10^{-4} N s/m^2 at 30^oC, whereas that of air 1.71×10^{-5} N s/m^2 at 0^oC, 1.76×10^{-5} N s/m^2 at 10^oC, 1.81×10^{-5} N s/m^2 at 20^oC, 1.86×10^{-5} N s/m^2 at 30^oC, and so on (Batchelor 1967). Thus, the value of μ can vary from 100 to 43 as temperature changes from 0^oC to 30^oC. To be consistent with $\rho_g = 1.25$ kg/m^3 taken at 10^oC, we use $\mu_g = 1.8 \times 10^{-5}$ N s/m^2 as the nominal value for air viscosity and $\mu = 75$ as a reference liquid-to-gas viscosity ratio.

4.1. The drop of $d = 800\,\mu m$

The experiments of Szakáll et al. (2009) (among others) showed that a drop with diameter $d = 800\,\mu$m exhibits a regular steady flow pattern of internal circulation without oscillations. So the drop with $d = 800\mu$m can serve as a test case for the present modeling effort.

In view of the present mathematical formulation, the solution is defined by the values of Re and Ca (or We) with given ρ and μ. Once the solution is computed and St is obtained as part of the solution which then yields C_D $(= 16\,St/(3\,Re))$, the corresponding drop size d and terminal velocity U can be determined according to the formulas (Feng 2010)

$$\begin{aligned} d &= \{3\mu_g^2\, Re^2\, C_D/[4\, g\, \rho_g^2\, (\rho - 1)]\}^{1/3} \\ U &= [4\, g\, \mu_g\, (\rho - 1)\, Re/(3\, \rho_g\, C_D)]^{1/3}\ . \end{aligned} \tag{11}$$

If we want to compute solution for a particular drop size, e.g., $d = 800\,\mu$m, we need to iteratively adjust the value of U for specifying Re and We until the value of d calculated from (11) converges to the target (e.g., $800\,\mu$m, as examplified next).

According to the formulas for terminal velocity derived by (Beard 1976, from various sources of theoretical and empirical information), a $800\,\mu$m drop should have $U = 3.225$ m/s with $Re = 179.164$ and $C_D = 0.8030$ (for $\rho = 800$, $\rho_g = 1.25$ kg/m^3, $\mu_g = 1.8 \times 10^{-5}$ N s/m^2, $\gamma = 0.07$ N/m, and $g = 9.8$ m/s^2), which can serve as the starting iterate for the present computation. With the values of Re and We being specified at 179.164 and 0.1486 ($1/Ca = Re/We = 1205.68$ for $\rho = 800$ and $\mu = 75$), the computed result shows that $St = 27.3022$ which leads to $C_D = 0.8127$, according to $16St/(3Re)$ in (10). From the known values of the computed C_D as well as other parameters, the drop diameter d and terminal velocity U obtained from (11) are 0.8032 mm (slightly larger than 800μm) and 3.2121 m/s (less than 3.225 m/s). After a couple of iterations by adjusting the value of U, the computed result at $Re = 177.133$, $We =$

[3]The actual computational code is called FECAW–Finite Element Computational Analysis Widget–as accessible from http://sites.google.com/site/jamesqfeng/

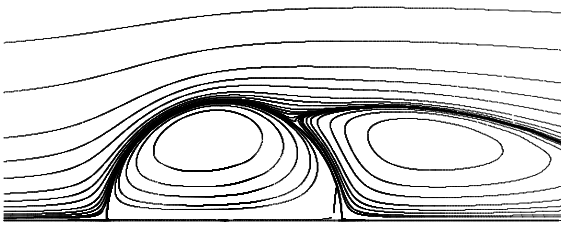

FIG. 2. Streamlines around a deformable drop (from $z = -2$ to $z = 3$) for $Re = 177.133$, $We = 0.1452$ corresponding to a water drop of $d = 0.8001$ mm with $\rho = 800$, $\mu = 75$, and surface tension $\gamma = 0.07$ N/m, at terminal velocity of 3.1881 m/s in air with density $\rho_g = 1.25$ kg/m^3, viscosity $\mu_g = 1.8 \times 10^{-5}$ N s/m^2. The contour values for streamfunctions shown here are 0, ± 0.0001, ± 0.0002, ± 0.0005, ± 0.001, ± 0.002, ± 0.005, ± 0.01, ± 0.02, ± 0.05, ± 0.1, etc.

0.1452 (for $U = 3.1884$ m/s) is found to yield $d = 0.8001$ mm and $U = 3.1881$ m/s from (11), and $C_D = 0.8218$ evaluated based on $16\,St/(3Re)$ as comparable to 0.8217 based on $8\,R\,g\,(\rho - 1)/(3\,U^2)$. Hence the present model by computing steady axisymmetric solution of the Navier-Stokes equations can provide all the detailed self-consistent description about a water drop of $d = 800\,\mu$m falling in air.

Figure 2 shows the streamlines of flow external and internal to the drop of $d = 800\mu$m, at $Re = 177.133$ and $We = 0.1452$. The pattern of internal circulation appears to agree well with that shown in a visualization photograph by Szakáll et al. (2009)[4]. The dimensionless value of the maximum internal circulation velocity (namely, the internal circulation intensity) v_{ic} is 0.0386 at polar angle $\theta = 67.5^o$ (measured from the front stagnation point) on the drop surface. This leads to an internal circulation velocity of 12.3 cm/s, very close to that reported by Szakáll et al. (2009).

From the resulting nodal coordinates along the drop surface, the axis ratio

$$\hat{\alpha} \equiv \frac{z_{max} - z_{min}}{2r_{max}} \tag{12}$$

can be readily determined for the $800\mu m$ drop as 0.9940, where z_{min}, z_{max} denote minimum and maximum z-coordinate values on the drop surface, and r_{max} is the radius of the drop cross-section (i.e., $2\,r_{max}$ represents the maximum transverse dimension). Hence the drop of $d = 800\,\mu$m has a nearly spherical shape with slight oblate deformation (with $\hat{\alpha}$ slightly less than unity).

[4] As discussed by Batchelor (1967), when the flow is steady, the streamlines coincide with the streak lines indicated by marking material in an experimental photograph

4.2. Drops of d between 1 mm and 1.5 mm

Falling at terminal velocity in air, a water drop of $d \geq 1$ mm is expected to oscillate with periodic vortex shedding in the unstable wake (cf. Beard 1976; Pruppacher and Klett 1978; Szakáll et al. 2009). Such drop oscillations tend to interrupt the regular steady internal circulation inside the drop and thereby reduce the overall internal circulation effect. Without undertaking the full three-dimensional transient simulations of the actual flow field, such a reduction of internal circulation effect may be accounted for by equivalently increasing the liquid viscosity μ in computing the steady axisymmetric flow. By comparing with the experimental information provided by Clift, Grace, and Weber (1978), the computational results of Feng (2010) suggest that $\mu = 200$ could be a reasonable choice for most of the cases with liquid drop falling in a quiescent gas, if better knowledge is unavailable. Therefore, we start with setting $\mu = 200$ in computing cases of a water drop of $d \geq 1$ mm with $\rho = 800$.

As exemplified in § 4.1 with a few iterations by adjusting U, we obtain a solution at $Re = 273.229$ and $We = 0.2765$ for $d = 1.0000$ mm and $U = 3.9344$ m/s with predicted $C_D = 0.6745$ and $\hat{\alpha} = 0.9821$ (assuming $\rho = 800$ and $\mu = 200$). As a reference, the terminal velocity for $d = 1$ mm according to the formula of Beard (1976) is 3.973 m/s and $\hat{\alpha}$ by Beard and Chuang (1987) 0.9841. The computed value of v_{ic} is 1.88×10^{-2} corresponding to a maximum value of steady internal circulation velocity of 7.41 cm/s. The computational result at $\mu = 200$ seems to predict a terminal velocity slightly ($\sim 1\%$) lower than that of Beard (1976) for the drop of $d = 1$ mm, as similar to that for the case of $d = 0.8$ mm in § 4.1 for $\mu = 75$. If the value of μ is reduced to 100, we obtain $U = 3.9601$ m/s and $\hat{\alpha} = 0.9876$. But the value of v_{ic} for $\mu = 100$ becomes 3.48×10^{-2}, which corresponds to a maximum value of steady internal circulation velocity of 13.8 cm/s that seems to be unreasonable because it exceeds the observed maximum value of the transient internal circulation velocity (Szakáll et al. 2009). Therefore, we decide to keep using $\mu = 200$ in the present work for lack of more accurate knowledge.

If the value of Re is set at 400, the computations (for $\rho = 800$ and $\mu = 200$) yield $d = 1.2113$ mm and $U = 4.7551$ m/s with $We = 0.2765$ and $C_D = 0.6745$. These results are still comparable to that from Beard (1976) at $Re = 400$ for $d = 1.2357$ mm and $U = 4.6614$ m/s, although the discrepancies grow from the cases of $d \leq 1$ mm especially for the value of terminal velocity. Indeed, Pruppacher and Klett (1978) suggested a cutoff point of $Re \sim 400$ for using the steady axisymmetric solutions to describe water drops falling in air.

Nevertheless, the computational solution can still be obtained for larger drops such as that of $d = 1.5$ mm at $Re = 614.906$ and $We = 0.9334$ with $U = 5.9031$ m/s, $C_D = 0.4494$, and $\hat{\alpha} = 0.9576$ (assuming $\rho = 800$ and $\mu = 200$). Compared with the prediction of Beard and Chuang (1987), i.e., $\hat{\alpha} = 0.9603$ for $d = 1.5$ mm, the present result for drop deformation seems to be quite reasonable. But the terminal velocity from Beard (1976) for $d = 1.5$ mm is 5.3275 m/s, about 10% less than the present computational result. This indicates inappropriate representation of the actual transient three-dimensional flow field using the steady axisymmetric solution when $Re \sim 600$, as commented by Pruppacher and Klett (1978). Thus, an alternative approach for computing the raindrop shape with $d \geq 1.5$ mm might be more desirable.

In view of the impressive success of previous models for the raindrop shape (Pruppacher and Pitter 1971; Beard and Chuang 1987; Beard, Feng, and Chuang 1989) by accounting only for the external aerodynamic pressure as the *net* flow effect based on that obtained at a fix value of Re, the most important parameter associated with the aerodynamic flow that significantly influences the drop deformation as the drop size changes appears to be the Weber number We, as explicitly shown in the nondimensionalized formulations of Beard, Feng, and Chuang (1989)[5]. The exact value of Reynolds number Re at which the aerodynamic pressure was measured does not seems to play a significant role on the drop shape evaluation. This is probably due to the fact that the drop deformation, when expressed in terms of Legendre polynomials or cosine series, behaves like a "low-pass" filter such that the drop deformation responses to the normal stress component associated with Legendre polynomial of degree n is demagnified by a factor of $(n^2 + n - 2)^{-1}$ (Beard, Feng, and Chuang 1989). If the normal stress distributions on drop surface at different values of Re mainly differ in the fine details represented by high-degree Legendre polynomials, the drop shape is not expected to change much as Re varies as long as the value of We is fixed. On the other hand, we realize that the steady axisymmetric solution cannot accurately represent the time-smoothed actual transient flow field for $Re > 400$ as indicated by the observed change of drag regime (cf. Pruppacher and Klett 1978). Therefore, it might be practically justifiable to disregard the value of Re that exactly matches all the physical properties (according to $2\rho_g\, R\, U/\mu_g$), and (iteratively) determine a value for Re such as to have a steady axisymmetric solution consistent with the drag coefficient $C_D = 8\, R\, g\, (\rho - 1)/(3\, U^2)$ and Weber number $We = 2\rho_g\, U^2\, R/\gamma$ for a given U and R. Hence, the drop shape, fluid dynamic stresses as well as hydrostatic pressure can be naturally adjusted self-consistently.

For example, when the value of Re is iteratively determined as 417.804 with the values of We and C_D specified at 0.7602 and 0.5518 (based on $\rho_g = 1.25$ kg/m^3, $d = 1.5$ mm, $U = 5.3275$ m/s, and $\gamma = 0.07$ N/m, with $\rho = 800$ and $\mu = 200$), the solution yield an axis ratio $\hat{\alpha} = 0.9586$ as quite reasonable in comparison with that of Beard and Chuang (1987). The computed value of v_{ic} is 2.22×10^{-2} corresponding to an internal circulation intensity of 11.8 cm/s, apparently very close to the maximum velocity observed by Szakáll et al. (2009) for a transient internal circulation. Thus, by computing solutions at a value of Re consistent with the specified values of We and C_D according to the given drop size d and corresponding value of U from Beard (1976), we may be able to predict raindrop shape for all drop sizes that are of practical interests without the need of further assumptions for explicitly adjusting aerodynamic pressure according to drop deformation as in Beard and Chuang (1987). Noteworthy here is that we must rely on the available knowledge about the terminal velocity as a function of drop sized (instead of predicting U as part of the solution computation), to model the steady axisymmetric raindrop shape with a self-consistent flow field, for drops of $d \geq 1.5$ mm. The steady axisymmetric flow field at $Re = 417.804$ may be considered as a reasonable approximation of the time-smoothed actual transient flow field at $Re = 2\rho_g\, R\, U/\mu_g = 554.9479$ for it at least yields the drag coefficient C_D that matches the measured value.

4.3. Drops of $d \geq 2$ mm

As described in § 4.2 for the case of $d = 1.5$, we now compute solutions for drops of $d \geq 2$ mm with $\rho = 800$ and $\mu = 200$ at specified values of U, We, and C_D provided in Table 1 for given d where the iteratively determined values of Re and the computed results for the internal circulation intensity v_{ic} and axis ratio $\hat{\alpha}$ are also listed.

The value of Re in table 1 for a given drop size d is generally smaller than that evaluated with $\rho_g\, d\, U/\mu_g$. This may be expected by realizing the fact that the time-smoothed governing equations for a transient flow usually contains Reynolds stresses (also known as "apparent" stresses) that effectively enhance the viscosity as a consequence of the additional *eddy viscosity* Schlichting (1968). Thus, the net effect of time-smoothing may be considered as to reduce the value

[5] Another apparently important parameter is the Bond number Bo, also known as Eötvös number Eo in (10); but it's associated with the hydrostatic pressure rather than the flow effect and it does not have direct influence to the drop deformation in the first-order perturbation equations (Beard, Feng, and Chuang 1989).

$d\,(mm)$	$U\,(m/s)$	We	C_D	Re	v_{ic}	$\hat{\alpha}$
2	6.4006	1.4631	0.5097	504.478	2.40×10^{-2}	0.9283
3	7.8846	3.3304	0.5038	569.180	2.60×10^{-2}	0.8528
4	8.6012	5.2843	0.5645	522.112	2.69×10^{-2}	0.7688
5	8.8390	6.9757	0.6682	436.632	2.71×10^{-2}	0.6837
6	8.8672	8.4243	0.7967	362.304	2.67×10^{-2}	0.6029
7	8.8655	9.8246	0.9298	312.418	2.63×10^{-2}	0.5262
8	8.9412	11.4207	1.0447	291.472	2.56×10^{-2}	0.4513

TABLE 1. Values of drop diameter d, terminal velocity U, Weber number We, drag coefficient C_D, Reynolds number Re, internal circulation intensity v_{ic}, and axis ratio $\hat{\alpha}$ determined by solving Navier-Stokes equations at specified values of We, C_D based on the values of U according to Beard (1976), with $\rho_g = 1.25$ kg/m^3, $\gamma = 0.07$ N/m, $\rho = 800$, and $\mu = 200$.

of Re by increasing viscosity. However, the eddy viscosity is not uniformly distributed like μ_g; it rather depends on the local eddy intensity. Strictly speaking, the nonzero eddy viscosity can only exist in the oscillatory wake region. Simply reducing the value of Re might at best be regarded as a first approximation that needs further verification by more thorough investigations.

Despite the drastically different approach, the value of axis ratio $\hat{\alpha}$ obtained with the present model agrees reasonably with that reported by Beard and Chuang (1987) up to $d \sim 5$ mm but deviates toward more severe drop deformation for larger d. In addition to $\hat{\alpha}$, the predicted maximum internal circulation velocity $v_{ic}\,U$ (e.g., 15.4, 20.5, 23.1, 24.0, 23.7, 23.3, and 22.9 m/s respectively for $d = 2$, 3, 4, 5, 6, 7, and 8 mm) seems to matche the observation of Szakáll et al. (2009) quite reasonably[6].

Figure 3 shows streamlines and shapes for water drops of $d = 2$, 4, 6, and 8 mm falling in air. With increase of drop size, the present model yields the drop shape closer to that of Beard and Chuang (1987) than the perturbation model (e.g., Pruppacher and Pitter 1971; Beard, Feng, and Chuang 1989). For example, figure 4 shows that for a drop of 5 mm the shape predicted by the present model (solid line) seems to differ very little from that of Beard and Chuang (1987) (dotted line), with the axis ratio $\hat{\alpha}$ differing by less than 4% (0.6837 versus 0.7080). Even at $d = 8$ mm, the flattened drop base does not seem to show a dimple predicted by the perturbation model for $d \geq 5$, being consitent with Beard and Chuang (1987). Physically, the occurrence of a dimple indicates a rapid change in drop's surface curvature that must be a consequence of a rapid change in the normal stress difference across the interface. Hence, the absence of a dimple suggests that the normal stress difference across the interface is likely to vary gradually rather than abruptly around the front stagnation point.

The plots of normal stress distribution shown in figure 5 indicate that the external normal stress, $-\,(4/Re)\boldsymbol{nn}\!:\!\boldsymbol{T}_g$, plays the major role in deforming the drop surface with its relatively large magnitude of variation; but the magnitude of variation of the internal (dynamic) normal stress, $-(4/Re)\boldsymbol{nn}\!:\!\boldsymbol{T}_l$, is not really negligible, although not as significant. Somewhat modified by the internal (dynamic) normal stress (especially noticeable for $d = 1$ mm), the plot of net dynamic normal stress distribution, $-(4/Re)\boldsymbol{nn}\!:\!(\boldsymbol{T}_g - \boldsymbol{T}_l)$, in figure 6 appears qualitatively similar to that of the external normal stress in figure 5. The combination of the net dynamic normal stress, the hydrostatic pressure $St\,z$, and the excess pressure p_a constitutes the total net normal stress. Multiplied by a factor of $We/4$, the total net normal stress becomes $Ca[\boldsymbol{nn}\!:\!(\boldsymbol{T}_g - \boldsymbol{T}_l) - St\,z + p_a]$, which equals the sum of the principal curvatures of drop surface–the term associated with $1/Ca$ on the right side of (3). The plot of sum of the principal curvatures in figure 6 shows that the curvatures around front and rear stagnation points ($\theta \sim 0^o$ and $\sim 180^o$) are reduced whereas that around equator ($\theta \sim 90^o$) enhanced from that of a sphere (with the sum of the mean principal curvatures equal to 2). Obviously, the drop of $d = 1$ mm has a nearly spherical shape with the sum of the mean principal curvatures differing little from 2, whereas the drops of $d = 2$ mm and 5 mm have local curvatures deviating from that of a sphere much more noticeably.

Unlike the external normal stress with the viscous stress component offering a negligible contribution (generally having a magnitude $< 1\%$ of that of the aerodynamic pressure), the internal (dynamic) normal

[6]The maximum values of internal circulation velocity reported by Szakáll et al. (2009) describe the time dependent flows with velocities varying from zero to the maximum values. Therefore, the maximum internal circulation velocity determined here for the equilibrium (or time-smoothed) flow field is expected to be somewhat less than the maximum value of Szakáll et al. (2009).

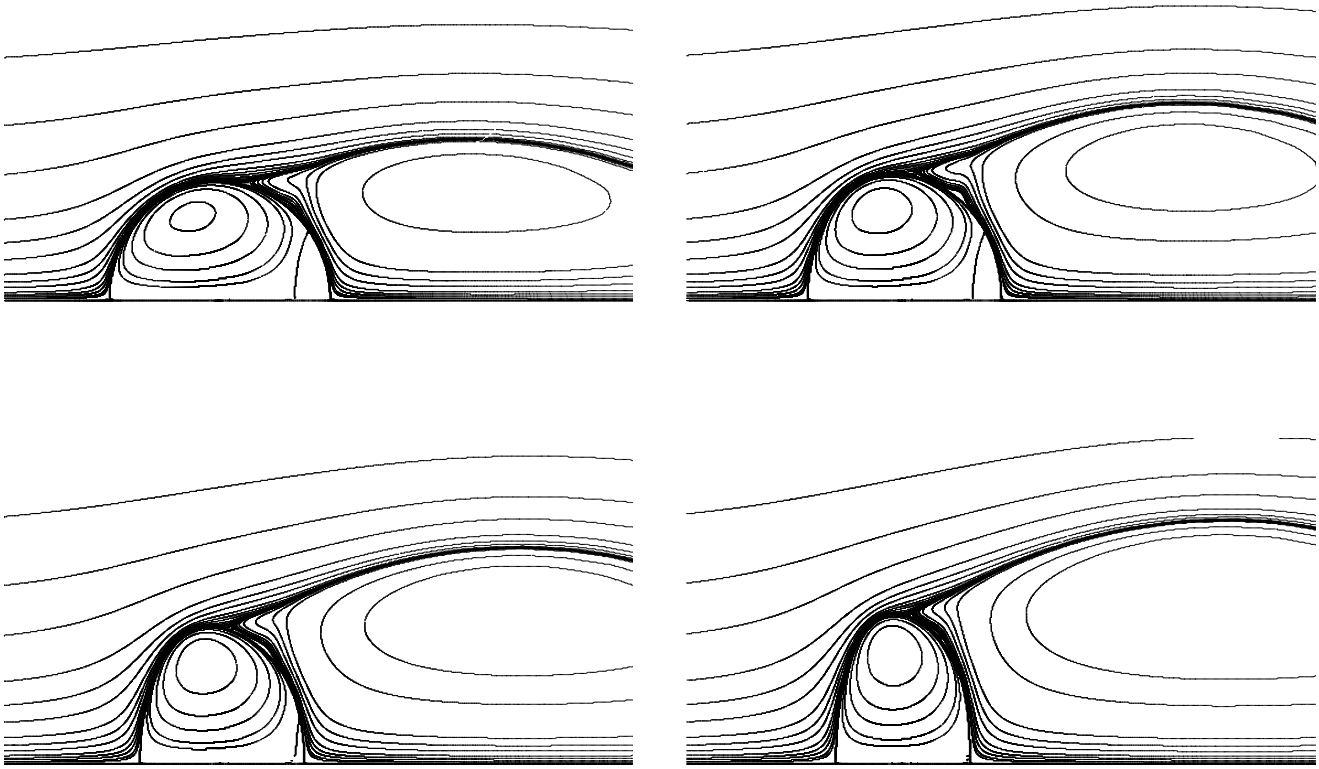

FIG. 3. Streamlines around deformable drops (from $z = -2$ to $z = 4$) for $We = 1.4631$, 5.2843, 8.4243, and 11.4207 and $C_D = 0.5097$, 0.5645, 0.7967, and 1.0447 corresponding to water drops of $d = 2$, 4, 6, and 8 mm with terminal velocity of 6.4006, 8.6012, 8.8672, and 8.9412 m/s in air. The numerical solutions are computed at the $Re = 504.478$, 522.112, 362.304, and 291.472 for specified values of We and C_D.

stress consists of both the pressure term and viscous stress component with comparable magnitudes. It seems the overall effect of the internal normal viscous stress component is to reduce the variation magnitude of the internal dynamic pressure due to internal circulation; thereby, the internal (dynamic) normal stress distribution along the free surface appears smoother with less variation magnitude than that of the internal dynamic pressure.

Figures 5 and 6 illustrate the fact that the net normal stress around the front stagnation point tends to spread to a larger area, rather than to concentrate in a region around $\theta \sim 0^o$, with increasing the drop deformation. Therefore, no sign of dimple formation at the front stagnation point even for very large drops (like that of $d = 8$ mm in figure 3). This is also consistent with the sum of the principal curvatures (as shown in figure 6) having positive values quite far from zero at $\theta = 0^o$.

In principle, the adjusted aerodynamic pressure of Beard and Chuang (1987) multiplied by an amplitude factor is an approximation to the net dynamic normal stress in a complete description of fluid mechanics as obtained with the present model. The aerodynamic pressure distribution used by Beard and Chuang (1987) was based on the measurement of Fage (1937) with a rather flat (i.e., almost constant) distribution on the rare surface of drop, in contrast to the present result with a gradual increase from equator to the rare stagnation point (cf. figure 6). Such an obvious difference in normal stress distributions seems to only result in a slight flattening of the drop surface around the rare stagnation point for the present shape comparing with that of Beard and Chuang (1987) (for $d = 5$ mm shown in figure 4). As discussed before, this is due to the fact that the drop deformation tends to diminish the "short-wavelength" effect, as indicated in the perturbation formulas in terms of Legendre polynomials (cf.

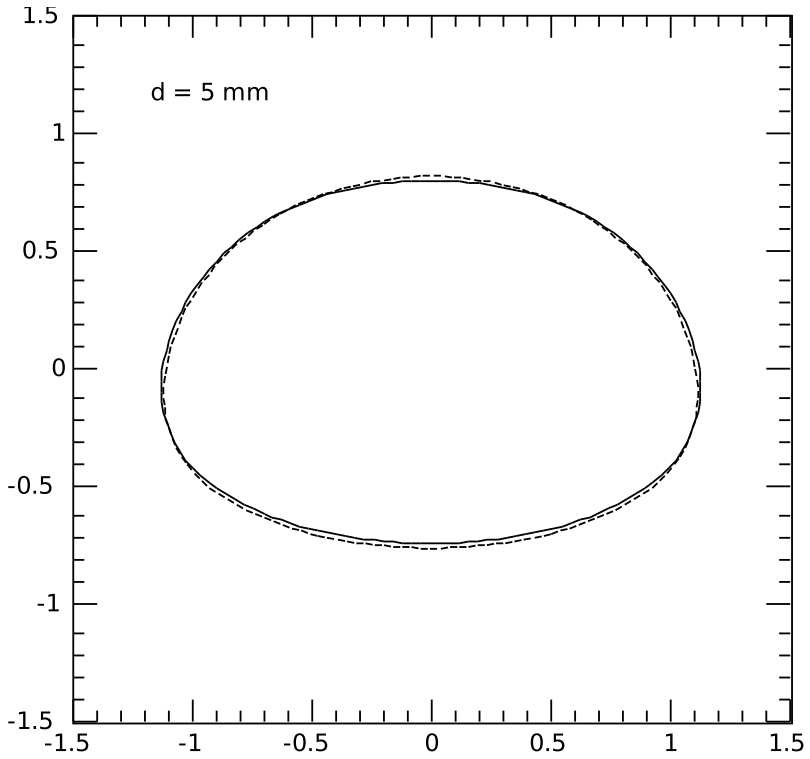

FIG. 4. Shape of the drop of $d = 5$ mm. Solid line–present model, computed at $Re = 436.632$ and $We = 6.9757$ ($= 436.632\,Ca$) with $\rho = 800$ and $\mu = 200$, and dotted line–the model of Beard and Chuang (1987).

Beard, Feng, and Chuang 1989) where the drop shape responds to the normal stress component associated with Legendre polynomial of degree n is demagnified by a factor of $(n^2 + n - 2)^{-1}$. Therefore, very similar raindrop shape can be obtained with models using noticeably different normal stress distributions, as long as the coefficients for low-degree Legendre polynomials are close enough. In fact, Beard, Feng, and Chuang (1989) showed that the axis ratio can be well approximated by using only the coefficient of Legendre polynomial of degree $n = 2$.

Figure 7 shows a comparison of axis ratio predicted by the present model and that of Beard and Chuang (1987), which can actually be fitted in simple formulas as

$$\hat{\alpha} = \begin{cases} 1 - 0.0159\,d^{2.2} & \text{for } d < 2 \text{ mm} \\ 0.0019\,d^2 - 0.0864\,d + 1.0942 & \text{for } d \geq 2 \text{ mm} \end{cases} .$$

The discrepancy becomes increasingly noticeable as drop size increases from $d = 4$ mm. However, the drop shape determined by the present model appears quite similar to that of Beard and Chuang (1987) even up to $d = 5$ mm (cf. figure 4 for the drop shape comparison of $d = 5$ mm), with only a slightly more flattening around the rear stagnation point. But for drops of $d > 5$ mm, the present result show a more severely deformed shape.

4.4. Cases at $20^o C$ and 1 atm

As might be noted, our nominal results presented so far are based on fluid properties at 10^oC and 1 atm (the standard sea level pressure). If the temperature is increased to 20^oC, as sometimes being considered in the literature (e.g., Beard 1976), we should have $\rho_g = 1.20$ kg/m^3 and $\rho = 829$, $\mu_g = 1.8 \times 10^{-5}$ N s/m^2 and $\mu = 55$. Based on these parameter values and following the procedure described in § 4.1, we can perform straightforward computations for the solution for a drop of $800\,\mu$m. The result shows that $U = 3.2393$ m/s, $C_D = 0.8249$, and $\hat{\alpha} = 0.9985$ at $Re = 172.7627$ and $We = 0.1439$, quite comparable to $U = 3.2596$ and $Re = 173.8461$ obtained from the formulas of Beard (1976). If the same parameter setting were applied to a drop of $d = 1$ mm, we would obtain $U = 4.0616$ m/s, $C_D = 0.6558$, and $\hat{\alpha} = 1.0046$–a prolate shape–at $Re = 270.773$ and $We = 0.2828$. This is consistent with the finding of Feng (2010) that prolate

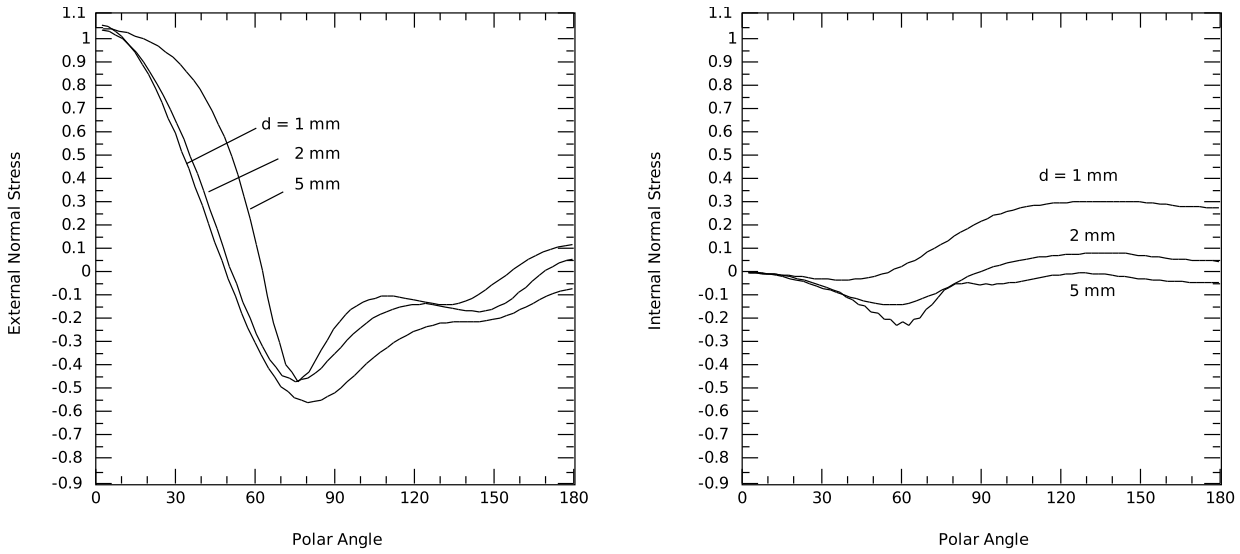

FIG. 5. Normalized external and internal normal stress distributions along the drop surface, $-(4/Re)\boldsymbol{nn}:\boldsymbol{T}_g$ and $-(4/Re)\boldsymbol{nn}:\boldsymbol{T}_l$ (which is shifted by a constant such that its value at $\theta = 0^o$ is zero), for cases of $d = 1$ mm ($Re = 273.229$, $We = 0.2765$), $d = 2$ mm ($Re = 504.478$, $We = 1.4631$), $d = 5$ mm, ($Re = 436.632$, $We = 6.9757$), with $\rho = 800$ and $\mu = 200$. Here the normal stress is normalized in such a way as to be consistent with the nondimensionalization of Beard and Chuang (1987); Beard, Feng, and Chuang (1989).

$d\,(mm)$	$U\,(m/s)$	We	C_D	Re	v_{ic}	$\hat{\alpha}$
2	6.4890	1.4437	0.5139	496.170	2.38×10^{-2}	0.9291
4	8.7515	5.2518	0.5651	519.502	2.67×10^{-2}	0.7709
6	9.0389	8.4036	0.7945	362.656	2.67×10^{-2}	0.6054
8	9.1041	11.3670	1.0443	290.034	2.56×10^{-2}	0.4544

TABLE 2. As in table 1 but with $\rho_g = 1.20$ kg/m^3, $\gamma = 0.07$ N/m, $\rho = 829$, and $\mu = 200$ (at 20^oC and 1 atm).

drop shape appears for $We < 10$ and $Re \geq 200$ when $\rho/\mu^2 > 0.15$ (because $\rho/\mu^2 = 0.274$ for $\rho = 829$ and $\mu = 55$.) But almost all the observations reported in the literature indicate a water drop falling in air with $d = 1$ mm has an oblate shape. Therefore, the solution with larger value of μ for $d \geq 1$ mm seems to be more reasonable for describing the drop deformation, because the vortex shedding induced drop oscillations tend to reduce the internal circulation intensity with a similar effect as increasing the liquid viscosity (cf. Feng 2010, and citations therein).

Following the similar approach described in § 4.2 with $\mu = 200$, we can compute a solution with $U = 3.9755$ m/s, $C_D = 0.6846$, and $\hat{\alpha} = 0.9824$–an oblate shape with $\hat{\alpha}$ comparable to that of Pruppacher and Pitter (1971); Beard and Chuang (1987); Beard, Feng, and Chuang (1989)–at $Re = 265.033$ and $We = 0.2709$ for $d = 1$ mm. Using the formulas of Beard (1976) would yield $U = 4.0087$ m/s and $Re = 267.245$ for $d = 1$ mm. As in § 4.3 for $d \geq 2$ mm, we can determine the drop shape by computing solutions with Re being determined for satisfying specified values of We and C_D according to a known terminal velocity U (e.g., from Beard (1976)) for a given d with $\rho = 829$ and $\mu = 200$. Table 2 shows the values of d, U, We, C_D, and iteratively determined Re, computed internal circulation intensity v_{ic}, and axis ratio $\hat{\alpha}$ at 20^oC and 1 atm. Because the corresponding value of We is slightly reduced at 20^oC from that at 10^oC in table 1, the axis ratio $\hat{\alpha}$ increases slightly for slightly less deformed drop. But the differences are so small (e.g., $< 1\%$) that the results for drop deformation at 10^oC and 1 atm may be considered to remain the same for 20^oC and 1 atm.

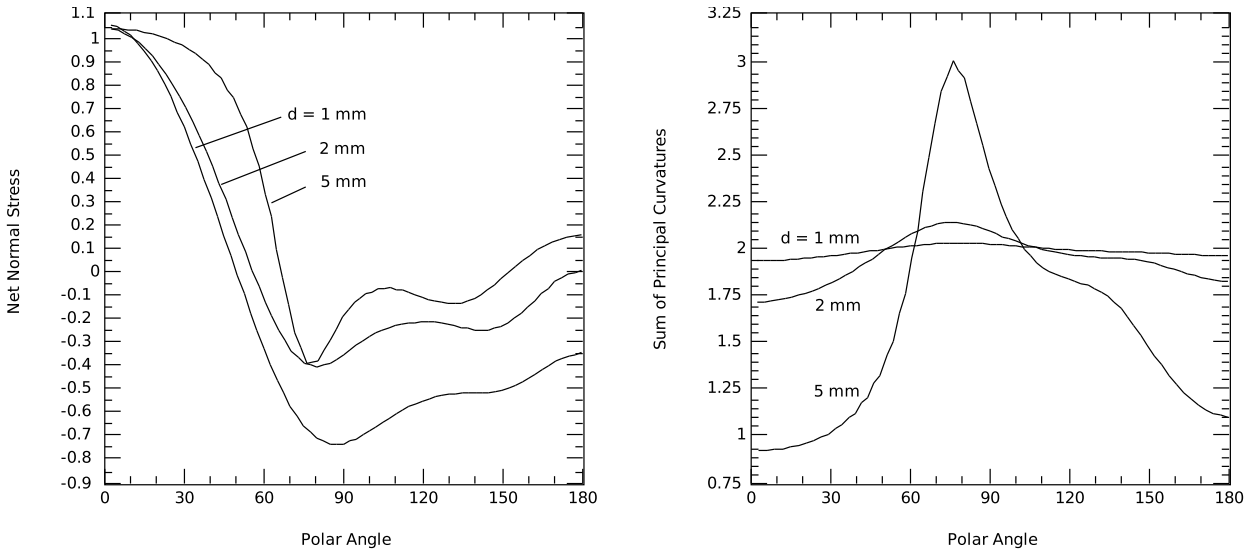

FIG. 6. Net dynamic normal stress distribution, $-(4/Re)\boldsymbol{nn}\!:\!(\boldsymbol{T}_g - \boldsymbol{T}_l)$, and sum of the principal curvatures, $Ca[\boldsymbol{nn}\!:\!(\boldsymbol{T}_g - \boldsymbol{T}_l) - St\, z + p_a]$, along the drop surface, for cases of $d = 1$ mm ($Re = 273.229$, $We = 0.2765$), $d = 2$ mm ($Re = 504.478$, $We = 1.4631$), $d = 5$ mm ($Re = 436.632$, $We = 6.9757$), with $\rho = 800$ and $\mu = 200$. Here the net dynamic normal stress distributions are shifted by a constant such that their values at $\theta = 0^o$ remain unchanged from that of the external normal stress.

$d\,(mm)$	$U\,(m/s)$	We	C_D	Re	v_{ic}	$\hat{\alpha}$
2	7.0706	1.4284	0.5222	479.792	2.33×10^{-2}	0.9313
4	9.5777	5.2418	0.5692	507.822	2.61×10^{-2}	0.7751
6	9.9155	8.4272	0.7966	357.738	2.62×10^{-2}	0.6116
8	9.9747	11.3708	1.0496	284.616	2.51×10^{-2}	0.4611

TABLE 3. As in table 1 but with $\rho_g = 1.00$ kg/m^3, $\gamma = 0.07$ N/m, $\rho = 1000$, and $\mu = 200$ (at 0^oC and 0.775 atm).

4.5. Cases at $0^o C$ and 0.775 atm

For a raindrop aloft, e.g., at 0^oC and 0.775 atm, we would have $\rho_g = 1.00$ kg/m^3, $\mu_g = 1.71 \times 10^{-5}$ N s/m^2, $\rho = 1000$ and $\mu = 100$. For a drop of $d = 800\,\mu$m, we obtain $U = 3.4867$ m/s, $C_D = 0.8599$, and $\hat{\alpha} = 0.9925$ at $Re = 163.1240$ and $We = 0.1389$, quite comparable to $U = 3.5389$ and $Re = 165.5606$ obtained from the formulas of Beard (1976). For a drop of $d = 1$ mm, we assume $\mu = 200$ with $\rho = 1000$ (as explained previously). The computational result indicates that $U = 4.3164$ m/s, $C_D = 0.7013$, and $\hat{\alpha} = 0.9824$ at $Re = 252.418$ and $We = 0.2662$, while the formulas of Beard (1976) would yield $U = 4.3615$ m/s and $Re = 255.060$.

For $d \geq 2$ mm, again we compute solutions following the same approach as in § 4.3 with $\rho = 1000$ and $\mu = 200$ according to specified values of U, We, and C_D given in table 3. The model predictions of the value of Re, the internal circulation intensity v_{ic}, and axis ratio $\hat{\alpha}$ at 0^oC and 0.775 atm shown in table 3 do not seem to vary much from that in tables 1 and 2, i.e., within $\sim 3\%$. Thus, our results for drop deformations at 10^oC, 20^oC and 1 atm are basically the same for drops aloft, as consistent with the findings of Beard (1976).

5. Discussion

By computing numerical solutions for steady axisymmetric flows governed by Navier-Stokes equations, we have demonstrated the model capability for describing the raindrop shape along with the associated flow field self-consistently. Except for relatively small drops of $d < 1$ mm, however, choosing parameter values for the computation do not appear straightfor-

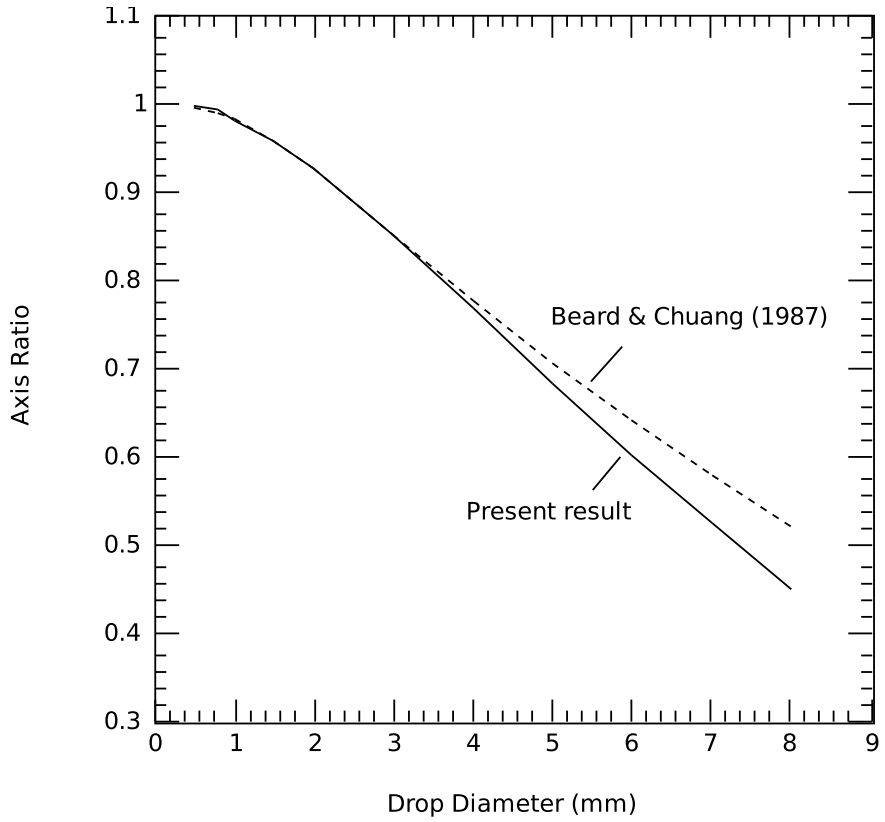

FIG. 7. Comparison of axis ratio predicted by the present model (solid line) and that of Beard and Chuang (1987) (dotted line).

ward, due to the nature of using the steady axisymmetric governing equations to determine the time- smoothed behavior of transient, three-dimensional flow field. For example, drops of $d \geq 1$ mm tend to have an unsteady wake with vortex shedding that triggers drop oscillations (cf. Beard 1976; Pruppacher and Klett 1978; Beard, Ochs, and Kubesh 1989; Szakáll et al. 2009). Hence, the regular internal circulation is interrupted with its time-smoothed intensity reduced as if the liquid viscosity is increased. Therefore, in computing the steady axisymmetric solutions of Navier-Stokes equations for describing the time-smoothed drop behavior, it is reasonable to set the viscosity ratio μ at a value greater than that evaluated with the viscosity values for water and air, e.g., to use $\mu = 200$ according to the findings of Feng (2010).

But when $d > 1.5$ mm and $Re > 600$, the model prediction of the drag coefficient C_D deviates noticeably from the experimentally measured value, indicating that the computed steady axisymmetric flow field cannot adequately describe the time-smoothed actual transient flow for $Re > 600$. Thus, we tried an approach by adjusting the value of Re so as to have computationally determined C_D and U match the experimentally measured values, while keeping the value of We fixed at that evaluated based on the experimentally measured terminal velocity U, for $\mu = 200$ and $d > 1.5$ mm. This approach seems to yield drop axis ratio comparable to the experimental data (described by the model of Beard and Chuang 1987) up to $d \sim 5$ mm, beyond which it consistently over-estimates the drop deformation (as shown in figure 7).

Considering the fact that evidence for setting $\mu = 200$ is not really that strong and the value of μ may offer another freedom for model adjustment, we then tried to allow both Re and μ to vary for matching the experimentally measured C_D, U, and $\hat{\alpha}$ (as given by Beard and Chuang 1987), again with the value of We kept fixed. The results so obtained are shown in table 4, with the values of $\hat{\alpha}$ varying no more than $\pm 1\%$ from that of Beard and Chuang (1987). Now with this approach, the only thing left for this model to predict seems to be the drop shape because even the axis ratio is given *a priori*. The drop shape predicted by this model for $d = 6$ mm is shown in figure 8, with that of Beard and Chuang (1987) presented in

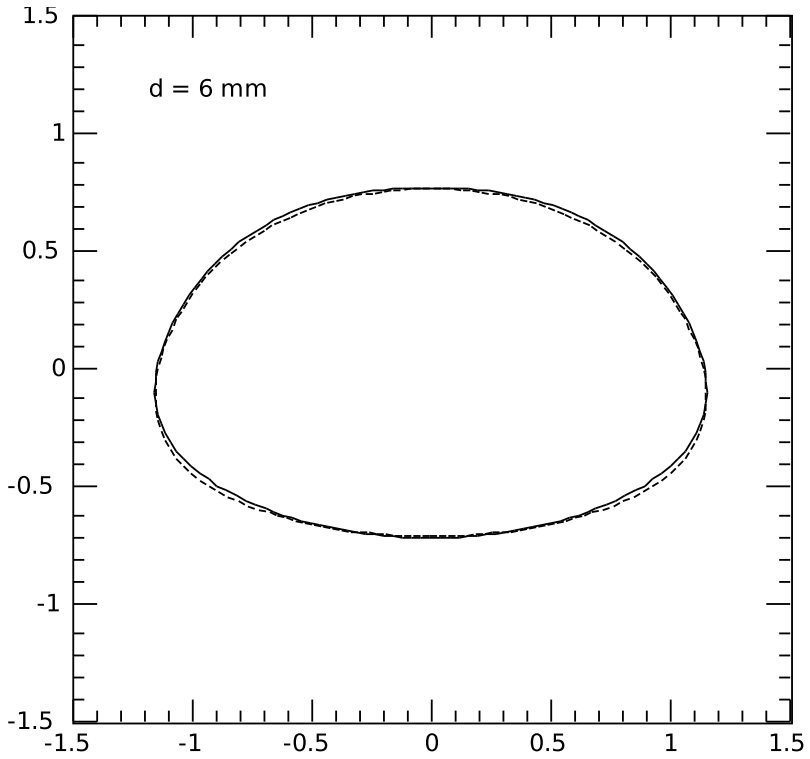

FIG. 8. Shape of the drop of $d = 6$ mm. Solid line–present model, computed at $Re = 339.234$ and $We = 8.4243$ $(= 339.234\,Ca)$ with $\rho = 800$ and $\mu = 130$, and dotted line–the model of Beard and Chuang (1987).

dotted line. Although the axis ratios are basically the same, a slight difference in drop shape can still be noticed between the present model and that of Beard and Chuang (1987). Although determining the proper value of μ by matching a given axis ratio $\hat{\alpha}$ seemingly compromises the prediction capability of the present model, it still demonstrates the intrinsic potential of this type of model for self-consistently describing the equilibrium deformable drop behavior even for drops of $d > 5$ mm despite the complexity of the actual transient flow field.

Another interesting finding is that the solutions computed at fixed $Re = 500$ with $\rho = 800$ and $\mu = 200$ for given values of We $(= 500\,Ca)$ in table 5 according to drop size d can predict the value of axis ratio as well as the drop shape quite comparable to those of Beard and Chuang (1987) for raindrops of practically all sizes. Despite the theoretical shortcoming for apparently incorrect C_D, computing solutions by this approach is much more straightforward without the need of iteratively adjusting either Re or μ. Here, this model with a fixed $Re = 500$ seems to be practically applicable for any raindrops of $d \geq 1.5$ mm as far as the drop shape is concerned. But the physical rationale for its validity is not obvious. At the present stage, it came about just fortuitously on a trial-and-error basis. Yet its practical success is too impressive to be ignored.

In principle, a complete description of the raindrop behavior can be achieved by computing the full three-dimensional transient solutions of Navier-Stokes equations. Then the 'equilibrium' raindrop shape can be obtained by a time-smoothing process over a large number of instantaneous solutions covering a long enough time period, which can also provide information about eddy viscosity distribution in the time-smoothed flow field, etc. However, such a rigorous approach is expected to be quite costly. One of the important findings in the present work is that despite the complexity of physical mechanisms, the 'equilibrium' raindrop shape seems to be rather insensitive to the fine details in the normal stress distribution, as theoretically illustrated in the perturbation equations of Beard, Feng, and Chuang (1989). Therefore, in the present work we explore the possibilities for self-consistently describing the time-smoothed raindrop behavior by computing steady axisymmetric solutions of Navier-Stokes equations, with the Reynolds stresses being accounted for

$d\,(mm)$	$U\,(m/s)$	μ	We	C_D	Re	v_{ic}	$\hat{\alpha}$
2	6.4006	200	1.4631	0.5097	504.478	2.40×10^{-2}	0.9283
3	7.8846	200	3.3304	0.5038	569.180	2.60×10^{-2}	0.8528
4	8.6012	180	5.2843	0.5645	515.938	2.91×10^{-2}	0.7754
5	8.8390	150	6.9757	0.6682	420.132	3.36×10^{-2}	0.7074
6	8.8672	130	8.4243	0.7967	339.234	3.68×10^{-2}	0.6448
7	8.8655	120	9.8246	0.9298	287.240	3.85×10^{-2}	0.5818
8	8.9412	110	11.4207	1.0447	258.574	3.93×10^{-2}	0.5263

TABLE 4. Values of drop diameter d, terminal velocity U, viscosity ratio μ, Weber number We, drag coefficient C_D, Reynolds number Re, internal circulation intensity v_{ic}, and axis ratio $\hat{\alpha}$ determined by solving Navier-Stokes equations at specified values of We, C_D based on the values of U according to Beard (1976), with $\rho_g = 1.25$ kg/m^3, $\gamma = 0.07$ N/m, $\rho = 800$.

$d\,(mm)$	$U\,(m/s)$	We	v_{ic}	$\hat{\alpha}$
2	6.4006	1.4631	2.39×10^{-2}	0.9280
4	8.6012	5.2843	2.67×10^{-2}	0.7648
6	8.8672	8.4243	2.80×10^{-2}	0.6461
8	9.9747	11.4207	2.81×10^{-2}	0.5401

TABLE 5. Values of given d, U, and We, with v_{ic} and $\hat{\alpha}$ determined by solving Navier-Stokes equaitons for $Re = 500$ with $\rho_g = 1.25$ kg/m^3, $\gamma = 0.07$ N/m, $\rho = 800$, and $\mu = 200$.

by simply adjusting the values of Re and μ. Our results show that self-consistent solutions can indeed be obtained with the raindrop shape, drag force, internal circulation intensity, etc. all in reasonable agreement with the experimental observations. But whether the adjusted values of Re and μ can be justified from the time-smoothed flow field and the eddy viscosity distribution in the actual three-dimensional transient flow is still open for future research.

Acknowledgement

The authors would like to thank Dr M. Szakáll and Dr S. Mitra of the University of Mainz for stimulating discussions.

REFERENCES

Aris, R., 1962 Vectors, Tensors, and the Basic Equations of Fluid Mechanics. Prentice-Hall.

Batchelor, G. K., 1967 An Introduction to Fluid Dynamics. Cambridge University Press.

Beard, K. V., 1976 Terminal velocity and shape of cloud and precipation drops aloft. J. Atmos. Sci., 33, 851-864.

Beard, K. V., Bringi, V. N., and Thurai, M., 2010 A new understanding of raindrop shape. Atmos. Res., ??, ??-?? (in press, doi:10.1016/j.atmosres.2010.02.001).

Beard, K. V. and Chuang, C., 1987 A new model for the equilibrium shape of raindrops. J. Atmos. Sci., 44, 1509-1524.

Beard, K. V., Feng, J. Q., and Chuang, C., 1989 A simple perturbation model for the electrostatic shape of falling drops. J. Atmos. Sci., 46, 2404-2418.

Beard, K. V., Ochs III, H. T., and Kubesh, R. J., 1989 Natural oscillations of small raindrops. Nature, 342, 408-410.

Blanchard, D. C., 1948 Observations on the behavior of water drops at terminal velocity in air. Gen. Electric Res. Lab., Occasional Report, No. 7, Project Cirrus, 13 pp. 1950 The behavior of water drops at terminal velocity. Trans. Amer. Geophys. Union, 31, 836-842.

Christodoulou, K. N. and Scriven, L. E., 1992 Discretiztion of free surface flows and other moving boundary problems. J. Comput. Phys., 99, 39-55.

Clift, R. C., Grace, J. R., and Weber, M. E., 1978 Bubbles, Drops and Particles. Academic.

Edgerton, H. E. and Killian, J. R., 1939 Flash! Seeing the unseen by ultra-high speed photography. Boston, Hale, Cushman and Flint, 203 pp.

Fage, A., 1937 Experiments on a sphere at critical Reynolds numbers. Aero. Res. Comm., England, Rep. and Memo. No. 1766, 20 pp.

Feng, J. Q. and Beard, K. V., 1991 A perturbation model of raindrop oscillation characteristics with aerodynamic effects. J. Atmos. Sci., 48, 1856-1868.

Feng, J. Q., 2010 A deformable liquid drop falling through a quiescent gas at terminal velocity. J. Fluid Mech., ??, ??-?? (in press).

Flower, W. D., 1928 The terminal velocity of drops. Proc. Phys. Soc. London, 40, 167-176.

Green, A. W., 1975 An approximation for the shapes of large raindrops. J. Appl. Meteor., 14, 1578-1583.

Hood, P., 1976 Frontal solution program for unsymmetric matrices. Int. J. Num. Meth. Engrg., 10, 379-399. [See ibid. 11, 1055 (1977) for corrigendum.]

Kistler, S. F. and Scriven, L. E., 1983 Coating flows. in Computational Analysis of Polymer Processing (ed. J. R. A. Pearson and S. M. Richardson), pp. 243-299. Applied Science.

Lenard, P., 1904 Uber regen. Meteor. Z., 21, 248-262. [for English translation see: 1905 Quart. J. Roy. Meteor. Soc., 31, 62-73.]

Magono, C., 1954 On the shape of water drops falling in stagnant air. J. Meteor., 11, 478-494.

Ortega, J. M. and Rheinoldt, W. C. 1970 Iterative Solutions of Nonlinear Equations in Several Variables. Academic.

Pruppacher, H. R. and Beard, K. V., 1970 A wind tunnel investigation of internal circulation and shape of water drops falling at terminal velocity in air. Q. J. Roy. Meteor. Soc., 96, 247-256.

Pruppacher, H. R. and Pitter, R. L., 1971 A semi-empirical determination of the shape of cloud and rain drops. J. Atmos. Sci., 28, 86-94.

Pruppacher, H. R. and Klett, J. D., 1978 Microphysics of Clouds and Precipitation. D. Reidel Dordrecht. 1997 2nd ed. Kluwer Academic.

de Santos, J. M., 1991 Two-phase cocurrent downflow through constricted passage. Ph.D. thesis, University of Minnesota.

Savic, P., 1953 Circulation and distortion of liquid drops falling through viscous medium. Natl. Res. Council. Canada, Rep. NRC-MT-22, 50 pp.

Schlichting, H., 1968 Boundary-Layer Theory. McGraw-Hill.

Strang, G. and Fix, G. J., 1973 An Analysis of the Finite Element Method. Prentice-Hall.

Szakáll, M.. Diehl, K., Mitra, S. K., and Borrmann, S., 2009 A wind tunnel study on the shape, oscillation, and internal circulation of large raindrops with sizes between 2.5 and 7.5 mm. J. Atmos. Sci., 66, 755-765.